NUCLEAR MAGNETIC RESONANCE: A NEW TOOL FOR THE VALIDATION OF MULTIPHASE MULTIDIMENSIONAL CFD CODES

H. Lemonnier

DTN/SE2T/LIEX, CEA/Grenoble, 38054 Grenoble cedex 9, France
Ph.: +33 (0)4 38 78 45 40, Fax: +33 (0)4 38 78 50 45, E-Mail: herve.lemonnier@cea.fr

Abstract

Turbulent transport models and data in bubbly flows are briefly reviewed since they play an important role in the modeling of boiling flows in forced convection. Shortcomings of earlier measurements of the eddy diffusivity by NMR (Lemonnier & Leblond, 2007b) are analyzed and a new procedure is presented which is now consistent with the procedure of Gatenby & Gore (1994) developed for single-phase turbulent flow characterization. The new estimate agrees with those obtained by Serizawa *et al.* (1975b) with a thermal method and with the model of Sato & Sadatomi (1981). This procedure also provides the liquid velocity fluctuation RMS and the Lagrangian correlation time of velocity fluctuations. In addition, the same NMR technique provides also the area-averaged liquid velocity and void fraction. Bubbly flow data up to transition to slug flow are provided which also agree with exiting drift-flux models (Ishii & Hibiki, 2006). It is finally discussed how the NMR method can be extended to local measurements and may provide a fully non intrusive diagnostic in two-phase flows and which is not limited to bubbly flow.

1 INTRODUCTION

It is believed that our understanding in many key issues of nuclear safety will no longer make any progress unless *validated* models are available. To quote only a few of them, PTS and convective boiling phenomena are two two-phase flow situations with heat transfer and phase change where turbulence plays a significant role and therefore should be modeled accurately.

Despite of the continuous growth of computing power, the progress of the development of two-phase turbulent transport models is still limited by our inability to determine experimentally the various quantities that appear in the closure relationships. Futhermore, many two-phase CFD approaches are no longer based on time- or ensemble-averaged quantities but on more complex time-space filtered quantities that are beyond the reach of local probe methods. It seems that NMR may provide a new insight into this field and it is the purpose of this paper to introduce this new field of research and to show how the modeling of two-phase turbulent transport phenomena can benefit from this technique.

NMR is a well known diagnostic tool in solid and liquid state physics as well as in chemical analysis. Its technological development has been boosted by its routine application to medical imaging and turn-key systems are now available that can also be applied to flow studies. Flow imaging is a routine diagnostic in medicine It is already possible to measure *in vivo* arterial blood flow rates, to determine the turbulent or laminar nature of blood flow and these techniques have been developed on dedicated experiments on pipe flows. Since two-phase flow occurs very seldom in biological fluids, the extension of these tools to two-phase gas-liquid or liquid-vapor flows have not been studied in detail. However, application to complex fluids rheology such as concrete and other multiphase dispersed media has been already attempted successfully. For a short review see for example Fukushima (1999).

In NMR, the fluid can be tagged by using its ability to be magnetized by applying a magnetic field. By using various auxiliary coils, it is possible to encode the magnetization with the fluid displacement or velocity and eventually get the probability distribution of the displacements or the velocities in the measuring volume. Moreover, the measuring volume can be shaped on purpose from a pipe length to a thin cross-sectional slice. The sensitivity within the probed volume can also be selected from the hardware only and can therefore be accurately controlled. By combining several of these one-dimensional

slicing techniques, it is possible to localize the measuring volume to any location within the flow and get space-filtered quantities that are usually involved in LES-like single- or two-phase flow models. For a review of basis principles of NMR see for example Callaghan (1991), Rodriguez (2004).

In this paper we will detail simultaneous measurements of the liquid mean velocity and void fraction in air-water two-phase pipe flows. It will be shown that in addition to the mean values, fluctuations can also be characterized. Since NMR is a purely Lagrangian method, dispersion can also be characterized directly and it will be shown that the turbulent eddy viscosity as well as the RMS of the velocity fluctuations can both be determined from the NMR signal. A very interesting by-product of the analysis is the Lagrangian integral scale that can also be deduced from the measurements. Most turbulent transport models are based on the eddy viscosity approach: NMR provide a direct determination of this parameter together with the time scale beyond which the diffusion limit of the turbulent mixing process is reached. Finally, it will be shown how selection (slicing) techniques can improve the space resolution of the measurement from the pipe cross section (presented here) to a small volume, leading to the possible development of a local diagnostic tool for two-phase flows.

2 MULTIDIMENSIONAL MODELING OF BOILING FLOW

There seems to exist a kind of general agreement on the form of local time-averaged equations that describe two-phase boiling flows (Delhaye *et al.* , 1981, Bergles *et al.* , 1981, Kataoka, 1986). There is also some agreement on the the decomposition of each variable into a mean value and its fluctuation (Kataoka & Serizawa, 1989, Ishii & Hibiki, 2006). However, boiling flow models differ mainly by their closure assumptions relative to,

- Wall related phenomena
- Turbulent transport in the bulk
- Interphase fluxes in the bulk

To quote one among other similar studies, the enthalpy equation of the Neptune code is reproduced only here for the sake of discussion, since the momentum equation has a similar structure (Mimouni *et al.* , 2008),

$$\frac{\partial}{\partial t}\alpha_k\rho_k\left(h_k+\frac{v_k^2}{2}\right)+\nabla\cdot\alpha_k\rho_k\mathbf{v}_k\left(h_k+\frac{v_k^2}{2}\right)=$$
$$\alpha_k\frac{\partial p}{\partial t}+\alpha_k\rho_k\mathbf{g}\cdot\mathbf{v}_k+\Gamma_k\left(h_{ki}+\frac{v_{ki}^2}{2}\right)+q"_{ki}A_i-\nabla\cdot\alpha_k(\mathbf{q}_k+\mathbf{q}_k^T) \quad (1)$$

where α is the phase time fraction, h is the enthalpy, $\mathbf{v}$ is the phase velocity, ρ is the density, p is the pressure, $\mathbf{g}$ is he specific gravity, Γ is the rate of phase production, $q"$ is the heat flux at the interface and $\mathbf{q}$, resp. $\mathbf{q}^T$ are the molecular heat flux and the turbulent heat flux and A_i is the interfacial area. The index k is relative to the phase and i to the values at the interfaces. Each phase variable is time- or weight and time-averaged as defined by Ishii & Hibiki (2006). We do not discuss here the various approximations leading to this equation but rather the modeling of the two main sources terms of the equation for the liquid phase:

- $\mathbf{q}_L^T$: the turbulent heat flux
- $q"_{Li}A_i$: the heat transfer at the interface

Turbulent momentum and heat transfer are usually modeled by a diffusion approach through an overall diffusivity coefficient decomposed according the initial scheme of Sato & Sadatomi (1981) in a contribution from shear induced turbulence and another from the bubble induced turbulence. Though it

is not detailed in general, analogy between heat and momentum transfer is assumed and both momentum and heat diffusivities are equal or proportional.

The heat transfer rate at the interface is modeled by known results on heat transfer on individual bubbles or drops. The temperature difference driving the transfer being the local subcooling or superheating of the liquid phase.

When subcooled boiling is analyzed with this model and a cup shaped liquid temperature profile is considered, at some distance from the wall, the saturation temperature is reached dividing the flow in a superheated region close to the wall where evaporation should occur and the subcooled bulk of liquid where condensation is expected. Clearly the interfacial heat transfer is a mechanism that must flatten the temperature profile towards thermodynamic equilibrium: superheated liquid provides heat to the interface, evaporation occurs and cooling results. On the other hand, subcooled liquid withdraw heat from interfaces and condensation occurs; as a result heat is released to the liquid. Turbulence acts in the same way since large temperature gradients increase the turbulent heat flux from the wall to the bulk. As a result, the flattening of the temperature profile is also expected from this latter mechanism.

It seems reasonable to think that with the knowledge of both the void fraction, temperature and velocity profiles for various inlet subcooling conditions, the contribution of each mechanism can be separated by using an extension of the analysis of Sato *et al.* (1981). Liquid velocity measurements in boiling flows being extremely scarce, it is difficult to directly assess even the order of magnitude of the turbulent shear stress or eddy diffusivity in the bulk. That is particularly unfortunate and large errors can be expected when trying to identify the respective contribution of turbulent heat flux and interfacial heat flux since both mechanisms act the same way: a defect in turbulent heat flux may be compensated by an excess of interfacial heat transfer.

It is therefore important to get an alternate access to the turbulent transport phenomena in order to allow a fair separation between the competing mechanisms.

3 EARLIER TURBULENT DISPERSION STUDIES

An indirect determination of the turbulent eddy viscosity in non vanishing void fraction conditions has been proposed by Sato & Sadatomi (1981). They analyzed different experiments in bubbly flow where both the void fraction and the liquid velocity profiles where known. By assuming the independency of shear stress and bubble induced fluctuations, they modeled separately these effects. Shear induced turbulence is modeled from known profiles of mixing length in single-phase pipe flow whereas bubble induced turbulence is assumed to be proportional to the bubble relative velocity, bubble diameter and void fraction. This was justified by an analogy with molecular mixing detailed in an earlier work (Sato & Sekoguchi, 1975).

Both mechanisms are damped down in the vicinity of the wall according to Van Driest suggestion (Sato & Sadatomi, 1981, eqs. 20 and 21). The shear stress definition together with the known value of the wall shear stress, provides an ODE in the liquid velocity, the profile of which can be derived. By fitting the constant in bubble induced eddy diffusivity, the following local estimate is obtained for the bubble induced diffusivity, ν_{TP},

$$\nu_{TP} = 1.2\alpha\frac{d_B}{2}U_B, \tag{2}$$

where d_B is a mean bubble diameter, U_B is the bubble relative velocity and the constant 1.2 is the best fit value obtained from the existing data and represent only a slight correction ($+20\%$) to the analytical estimate of (Sato & Sekoguchi, 1975). Note that a similar approach is developed by Sato & Sadatomi (1981) for predicting temperature profiles in vertical bubbly flow under constant heat flux conditions.

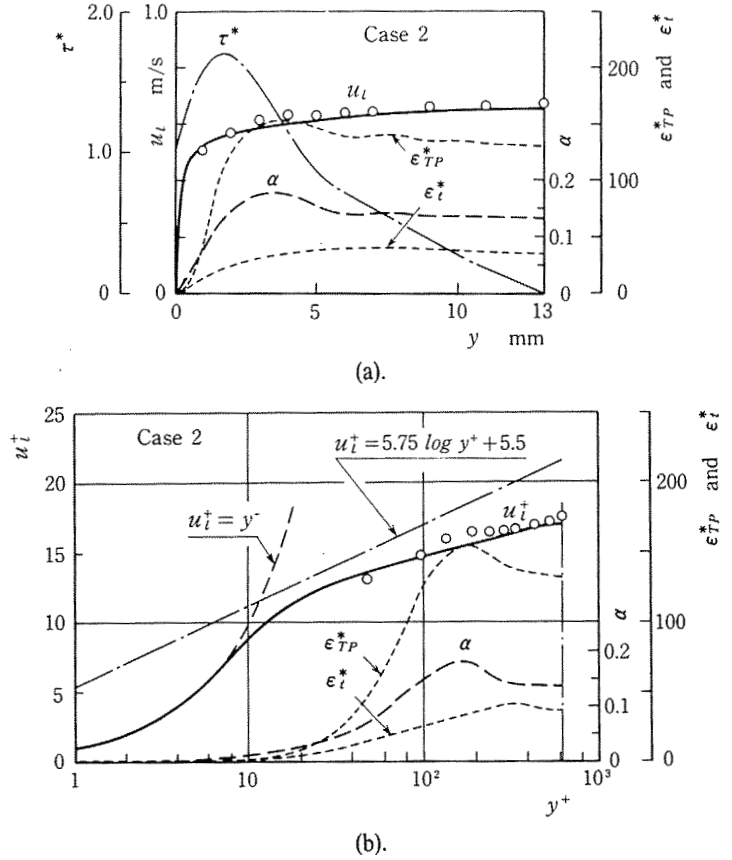

Figure 1: (a) Distribution of the non dimensional shear induced diffusivity, ϵ_l^*, two-phase diffusivity, ϵ_{TP}^*, void fraction α and liquid velocity, u_l after (Sato *et al.* , 1981, fig. 4). In subfigure (b), velocity and distance from the wall, y are expressed in wall units. Bubbly flow, $J_L = 0.5$ m/s, $J_G = 0.105$ m/s, $P = 1.31$ bar, $\langle \alpha \rangle_2 = 0.131$, $D = 26$ mm, $b_B = 4,8$ mm.

The temperature profile is predicted from the turbulent heat flux definition and the known value of the wall heat flux.

It is remarkable to note that predicted distribution of the turbulent diffusivity is rather flat in the bulk and that both the shear induced and bubble induced turbulent diffusivity are (i) much larger than the molecular diffusivity ($\epsilon^* = \nu/\nu_L$) and (ii) for void fraction as small as 10%, the bubble induced turbulence is the predominant effect. This also suggests that bubble induced turbulent is rather homogenous in bubbly flow which was later confirmed by the direct measurement of liquid velocity fluctuations (Liu & Bankoff, 1993, Grossetête, 1995) .

Serizawa *et al.* (1975b) studied experimentally the thermal mixing and bubble dispersion in bubbly flow by using two original approaches : the analysis of the thermal wake of a thin heated rod and the distribution of helium in gas bubbles downstream a point source.

By assuming that the liquid is tagged with the temperature, the temperature distribution is a direct measure of the Lagrangian displacement of the liquid. Space to time conversion is done assuming a constant mean liquid velocity in the bulk of the liquid and the RMS of the mean lateral displacement $[X^2]$ at time Δ is obtained from the second order moment of the temperature distribution. These authors refer to earlier work by Hinze based on the seminal study by Taylor (1921, Eq. 23) which relates the variance of the lateral displacements to the liquid velocity fluctuations RMS by,

$$[X^2] = 2[u^2](T_0\Delta - T_0^2(1 - \exp(-\Delta/T_0))) \tag{3}$$

where T_0 is the Lagrangian time scale of turbulence, defined from the velocity Lagrangian correlation

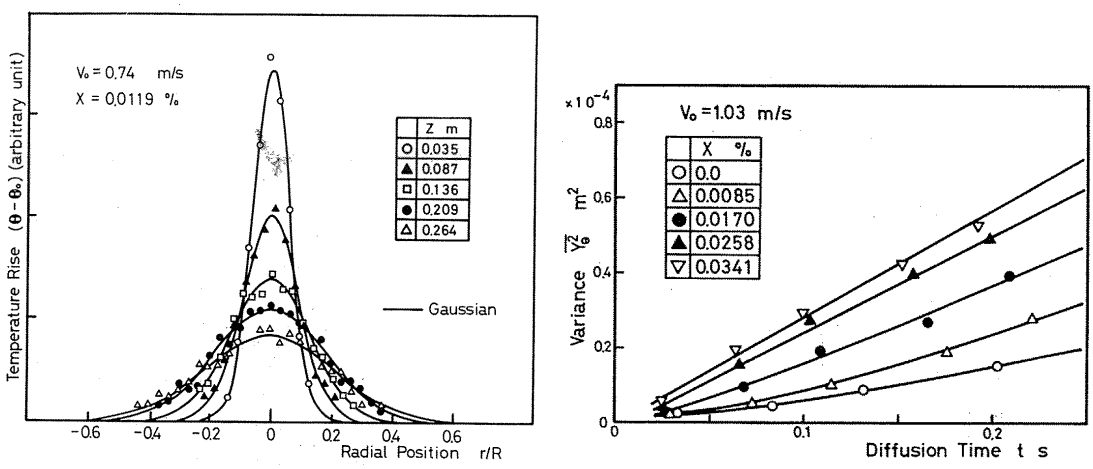

(a) Thermal wake at various downstream distances (b) RMS of temperature profile *vs* transit time

Figure 2: Analysis of the thermal wake behind a heat rod in bubbly flow, various conditions. Pipe diameter, $D = 60$ mm. After Serizawa *et al.* (1975b, Figures 1 and 2).

and the bracket denotes the statistical average. This model predicts that the variance of fluid lateral displacement is quadratic for short times ($\Delta \ll T_0$) and linear for long times. Taylor (1921) further showed that the diffusion coefficient can be directly deduced from the displacement variance,

$$D = [uX] = \frac{1}{2}\frac{\mathrm{d}}{\mathrm{d}\Delta}[X^2] = [u^2]T_0\,(1 - \exp(-\Delta/T_0)) \tag{4}$$

This results shows that for long times, D tends asymptotically towards $[u^2]T_0$ and is less than this value for short times. The diffusivity for short times behaves as $[u^2]\Delta$. At this scale velocity fluctuations are strongly correlated. An estimate of the correlation time can be calculated from the time a fluid particle sees two successive bubbles L_B/U_B where L_B is the mean distance between bubbles and U_B is the bubbles relative velocities. L_B can also be replaced with d_B the mean bubble diameter. For bubble velocities of the order 25 cm/s, this two times range between 10 to 50 ms. The two trends of the variance are clearly visible in figure 2(b), in particular for low void fraction values, whereas at higher void fraction, the linear behavior is only visible. This figure also shows that dispersion is an increasing function of quality (or void fraction) at a given liquid superficial velocity and that the correlation time of turbulence seems to be a decreasing function of void fraction. Serizawa *et al.* (1975b) did not interpret the integral scale but rather correlated the diffusivity with the Lockhart-Martinelli parameter X_{tt} rather successfully.

However, from the data of figure 2(b), it is clearly visible that the order of magnitude of T_0 is 10-100 ms. This time represents the time scale beyond which the *diffusion limit* is reached and therefore, the time scale over which turbulence mixing can legitimately be modeled by diffusion. This is to the author knowledge the very first physical argument that can justify the choice of the averaging time for the time-averaged balance equations.

It is well known in NMR community that molecular diffusivity can be measured from the decay of magnetization (Callaghan, 1991). Stejskal & Tanner (1965) first showed how this decay is related to self-diffusivity resulting from molecular Brownian motion. To make a long story short, a physical image of the measurement is described in detail in Lemonnier & Leblond (2007b). A still fluid sample is tagged with magnetic fringes, almost instantly. Then after a time Δ, the magnitude of these fringes is read from a magnetization measurement. The fringe pattern fades away with time due to molecular mixing during the time Δ and from the observation of the decay rate, the molecular diffusion can be

deduced. It is worth noting that with this non intrusive measurement, it is possible to investigate the dispersion phenomenon at a given length scale (fringe spacing) and a given time Δ. Both scales can be set independently.

Another interpretation of the measurement by using the so-called PFGSE[1] sequence is the following relation between the magnetization or NMR signal and the fluid displacement distribution within the magnetized volume,

$$S(g) = \int_{-\infty}^{\infty} p(v) \exp(i\gamma g \Delta \delta v)\, \mathrm{d}v \tag{5}$$

where the product, Δv, is the mean displacement during time Δ, v is the mean velocity during time Δ, g is the pulse gradient strength, δ is its duration and γ is a constant physical property of protons (nuclear gyromagnetic constant). The magnetic fringe spacing, λ, is inversely proportional to the product $g\delta$ and S appears to be the Fourier component of the displacement distribution at the length scale λ. The most relevant consequence of (5) is that the displacement distribution is the inverse Fourier transform of the measured NMR signal at the end of the PFGSE sequence. It can therefore be determined experimentally. The direction of the displacement can be selected from hardware: both the transverse or longitudinal displacements can be measured.

From the displacement distribution at time Δ, the Lagrangian centered variance of fluid displacement can be determined $[(X - [X])^2]$. In fully developed pipe flow $[X]$ is zero for lateral motion and is proportional to the area-averaged liquid velocity for longitudinal motion (Tennekes & Lumley, 1972, Ch. 7). This latter point will be shown later in this paper and is the base of the velocity measurement.

Gatenby & Gore (1994) extended the molecular diffusivity measurement to eddy viscosity measurement in turbulent single-phase pipe flow and grid turbulence spatial decay. NMR measurements were found to agree with known trends. These authors based their analysis both on the analysis by Taylor (1921) and some reworking of the theory of Stejskal & Tanner (1965) accounting for the time dependency of dispersion. Lemonnier & Leblond (2007b) used this technique and analyzed the longitudinal displacement centered variance and by an approximate reasoning produced eddy diffusivity estimates, which agree only qualitatively with Serizawa's earlier estimates, see Figure 3.

In Figure 3, orders of magnitude are consistent ($D \approx 5\,10^{-5}$ m^2/s). Next Diffusivity is seen to be an increasing function of void fraction as expected from the earlier analysis by Sato & Sadatomi (1981), see (2). Finally as expected from this latter result, diffusivity seems to depend mainly on void fraction rather than gas quality. From the slope of $D(\alpha) = 1/2\alpha d_B U'_B$, the magnitude of the product $d_B U'_B$ can be estimated to $5\,10^{-5}$ m^2/s. A rough estimate of the bubble diameter from flow snapshots was 4 mm, which leads to a value of $U'_B \approx 12.6$ cm/s in agreement with the order of the magnitude of slip velocity in these conditions (25 cm/s). This estimate is however lower than expected which is consistent with generally weaker diffusion coefficient estimated by NMR compared to the thermal method. This will be further discussed in this paper.

Serizawa's data is limited to vertical bubbly flow whereas data by Lemonnier & Leblond (2007b) extends to bubble clustering regime close to the bubble-slug transition ($\alpha > 20\%$). It is therefore striking to see the impact of the change in flow regime: at low void fraction, liquid agitation is moderate and result from the individual bubble random motions, whereas at higher void fraction values, observation shows that liquid agitation is tremendously increased by formation of large scale wakes behind bubble clusters ($[u^2]$ increases visibly).

However, the analysis by Lemonnier & Leblond (2007b) suffered from several shortcomings. Longitudinal displacement distributions were analyzed instead of those of the lateral displacement, which

[1] PFGSE: pulsed field gradient spin echo, see for example Callaghan (1991)

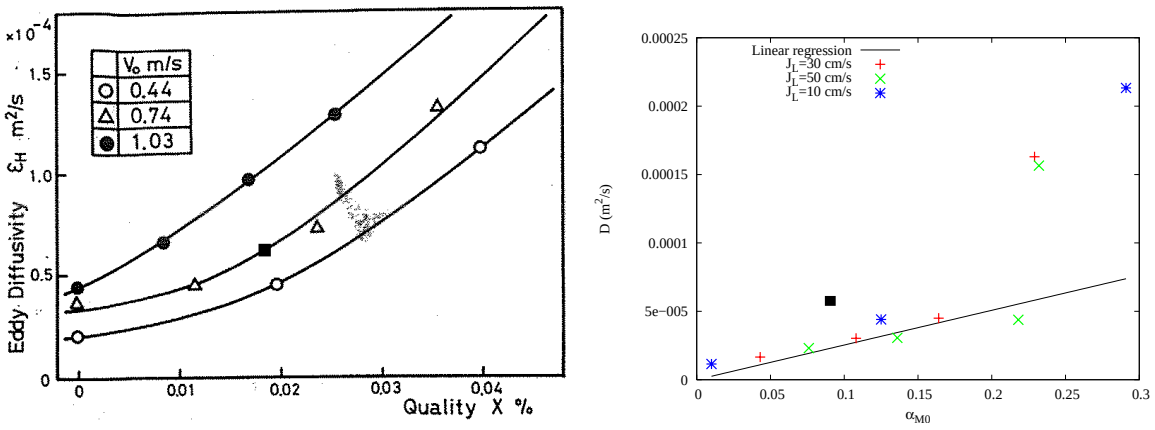

(a) Two-phase eddy diffusivity, thermal method

(b) Two-phase eddy diffusivity by NMR

Figure 3: Comparison of the two-phase diffusivity measured in bubbly flow with the thermal method of Serizawa *et al.* (1975a) and NMR approximate procedure of Lemonnier & Leblond (2007b). Pipes diameter and mean liquid velocities are similar, $D = 60, 49$ mm and $J_L = 0.5 - 1$ m/s and 0.1-0.5 m/s respectively.

would have been fully consistent with Serizawa's analysis. In addition, Taylor's analysis legitimately applies only to lateral motions and as shown by Tennekes & Lumley (1972, Ch. 7), the cross sectional averaged centered variance of the longitudinal displacement in fully developed flow and homogenous turbulence is determined both by the spatial distribution of mean velocity in the pipe cross section and the liquid velocity RMS. It is however expected that with increasing void fraction, the latter effect becomes dominant. Furthermore, at the time this data was taken, no care was taken to verify whether the diffusion limit was reached in the measurements and Δ was selected in the 5-10 ms range with no further justification.

4 NMR STUDY OF DISPERSION IN BUBBLY FLOW

In order to be consistent with Serizawa's analysis, it was decided to analyze in depth the dependency of the variance of the lateral displacement with the time lag, Δ. This is directly possible since the PFGSE sequence provide exactly the displacement distribution at time Δ.

Sample NMR data in bubbly flow is shown in Figure 4. From the displacement distribution (see Figure 4(b), the variance of the displacement can be obtained. Two methods were used: (i) the direct calculation of the variance from the distribution,

$$[X^2] = \frac{\int_{-\infty}^{\infty} x^2 p(x)\,\mathrm{d}x}{\int_{-\infty}^{\infty} p(x)\,\mathrm{d}x} \tag{6}$$

where the denominator acts as a normalization constant. (ii) The second method is the fitting of a Gaussian. Both methods generally agree, the latter being used for simplicity. Next Δ is varied. The corresponding results are shown by the red crosses in figure 5(a). It is striking that the trend predicted by Taylor (1921) is clearly observed (see Eq. 3). By fitting $[u^2]$ and T_0 to this data, the following numerical values are obtained,

$$u' = \sqrt{[u^2]} = 7.89 \text{ cm/s}, \quad T_0 = 9.46\text{ms} \tag{7}$$

With this fitted parameter values, (3) represents fairly well the data of Figure 5(a). The correlation time T_0 is of order of 10 ms which is consistent with the data of Serizawa shown in figure 2(b) where the diffusion limit seems already reached at 20 ms for comparable void fraction. From the known values

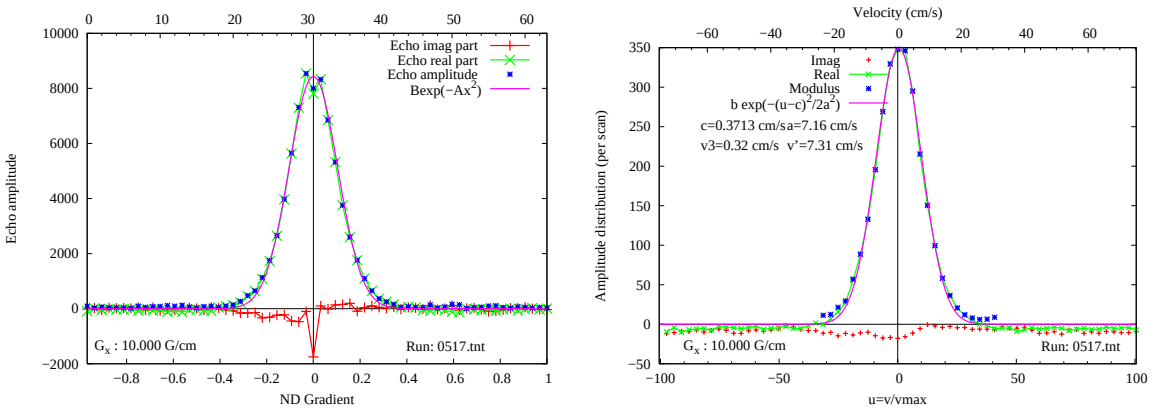

(a) Magnetization decay

(b) Lateral motion distribution

Figure 4: Sample NMR data in bubbly flow, $J_L = 30.3$ cm/s, $J_G = 4.87$ cm/s, $R_{G3} = 8.7$ %, $p \approx 1.2$ bar. Run 0517, $\Delta = 5$ ms. (a) Signal decay as a function of gradient strength, (LHS of eq. 5), (b) $p(v)$ obtained by inverse Fourier transform of data (a). Velocity to displacement conversion is simply $v\Delta = x$.

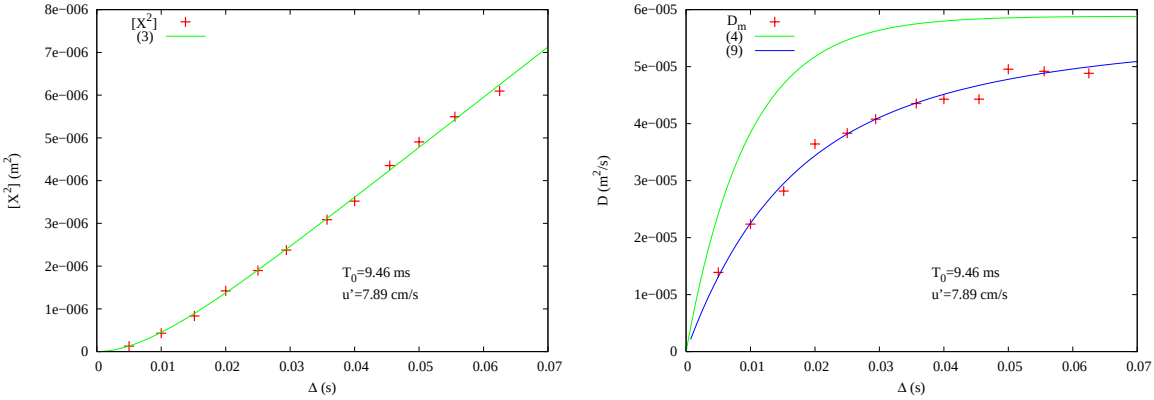

(a) Variance of lateral motion

(b) Dispersion coefficient

Figure 5: (a) Variance of lateral motion versus time lag Δ. Two-phase vertical bubbly flow, $J_L = 30,3$ cm/s, $J_G = 4,87$ cm/s, $R_{G3} = 8,7$ %. Runs 0517 to 0529, $\Delta = 5$ to 62,5 ms, $\delta = 1$ ms.

of the constants, Taylor's estimate of the dispersion coefficient can be calculated by using (4). The result is shown in figure 5(b).

From figure 4(a), the signal decay with the increasing value of the gradient strength can be analyzed. Stejskal & Tanner (1965) theory is applied and an estimate, D_m of the eddy diffusivity also be determined. Theory predicts a Gaussian shape for magnetization decay, the width of the Gaussian being proportional to D_m.

$$S(g) = S(0)\exp(-\gamma^2\delta^2 D_m(\Delta - \delta/3)) \tag{8}$$

As shown in Figure 4(a), the Gaussian behavior is observed and by curve fitting, D_m can be obtained. The corresponding values are shown by the symbols in figure 5(b). It is clear that estimates of D_m agree only qualitatively with Taylor's theory (4). By further comparing our magnetization decay analysis based on Stejskal & Tanner (1965) result and that of Gatenby & Gore (1994), it is found that the short time behavior disagrees by a factor of two whereas the long time trend agrees. Moreover, Stejskal & Tanner (1965) result was developed for molecular diffusion studies were the diffusion limit is always

reached and therefore D is assumed to be a constant. When D varies on a time scale comparable to T_0, this simple theory no longer applies. However, the analytical solution procedure of the magnetization diffusion problem (Stejskal & Tanner, 1965) can still be applied and, in the limit of very short gradient pulses, $\delta \ll \Delta$, it can be shown that D_m actually measured by magnetization attenuation (8) is simply the time averaged value of D over time Δ. By averaging Taylor's result on time Δ, the following expression is obtained for D_m,

$$D_m = \frac{1}{\Delta}\int_0^{\Delta} [u^2]T_0(1-\exp(-\Delta/T_0))\mathrm{d}\Delta = [u^2]T_0\frac{\Delta - T_0(1-\exp(-\Delta/T_0))}{\Delta} \tag{9}$$

The asymptotic trends of this new model agree with that of Gatenby & Gore (1994) in the limit of vanishing values δ/Δ, which is the case in our experiments ($\delta = 1$ ms). As a consequence, the experimental determination of D_m in figure 5(b) should be compared with (9) instead of (4). Figure 5(b) shows that data agrees very satisfactorily with our simple extension of the theory of Stejskal & Tanner (1965) which also agree asymptotically with the earlier theoretical results of Gatenby & Gore (1994).

For the sake of completeness, the value of the asymptotic diffusion is calculated, $D = [u^2]T_0 \approx 5.9\,10^{-5}$ m^2/s and is shown in Figure 3(a) ($X = 1.9\,10^{-4}$) and in Figure 3(b) as a black square symbol. This new estimate lies within the data of Serizawa and is much larger than the earlier estimates by Lemonnier & Leblond (2007b). This can be easily understood since the earlier data was taken at $\Delta = 5$ ms, well below T_0. Finally, this value compares favorably with Sato's equation (2) which provides $D = 5.2\,10^{-5}$ m^2/s with a bubble diameter of 4 mm and a bubble velocity of 25 cm/s.

5 LIQUID VELOCITY LIQUID FRACTION MEASUREMENTS

As shown earlier by Leblond *et al.* (1994, 1998) with the same spectrometer described in detail by Javelot (1994), area-averaged velocity and void fraction can be determined from the NMR signal with the PFGSE sequence. The absolute magnitude of the signal is proportional to the liquid content of the magnetized volume. By comparing single-phase signal to two-phase signal magnitude, it is possible to determine directly the liquid content of the magnetized volume also called here the control volume. These later concepts are left vaguely defined here and will be discussed later in this paper. The flow under investigation being nearly fully developed, the precise longitudinal extension of the measuring volume has no consequences on the interpretation of the measurements.

This ideal situation does not take into account the natural magnetization relaxation. Magnetization of the liquid is obtained by applying a uniform and constant magnetic field (≈ 0.12 T) on the flow. For various physical reasons, magnetization is not permanent but rather relaxes towards equilibrium according to a first order linear relaxation law. Relaxation times can be determined directly by using particular sequences (Callaghan, 1991) and it is sufficient to know here that their magnitude is 2 s for water. As a result, with an electromagnet of finite length, magnetization at the measuring section depends slightly on the liquid velocity. A simple model can be derived (Lemonnier & Leblond, 2007a) and leads to the following relation,

$$S = S_\infty\left(1-\exp\left(-\frac{L}{J_L T_1}\right)\right) \tag{10}$$

where L/J_L is the transit time of the liquid in the bore of the electromagnet of length L and S_∞ is the signal at the fully polarized conditions. Figure 6(b) shows the experimental trend is correctly predicted by (10). In addition curve fitting provides a longitudinal relaxation time estimate, $T_1 \approx 2.6$ s, in close agreement with the known value 2.4 s (Carr & Purcell, 1954). It is worthwhile mentioning that the sensitivity of magnetization to transit time and therefore to the mean fluid velocity can be used to meter fluid (see Daalmans *et al.* , 2007, figure 7).

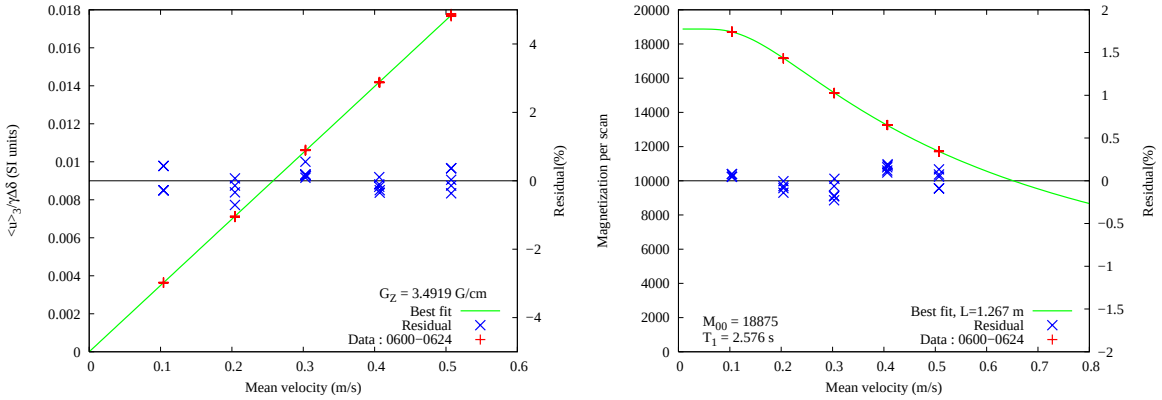

(a) Gradient calibration

(b) Magnetization calibration

Figure 6: (a) Reduced mean velocity, $\langle u \rangle / \gamma \delta \Delta$, as a function of the measured superficial velocity. (b)Magnetization variation at the measuring volume with respect to the fluid mean velocity in single phase flow. Runs 0600-0624.

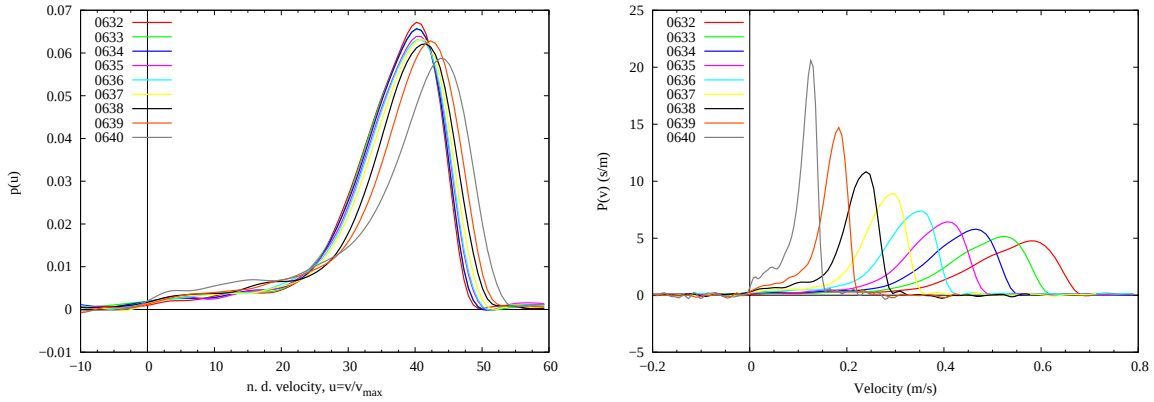

(a) Non dimensional velocity distributions

(b) Velocity disributions

Figure 7: Single-phase velocity ditribution. Superrficial velocity J_L ranging from 10 to 50 cm/s. Runs 0632-0640, $G_Z = 3.4919$ G/cm.

For various technological reasons, the gradient strength is only known in magnitude and reference measurements must be performed to get a calibrated value. Usually a molecular diffusion measurement is used, we preferred a direct comparison of the mean displacement measured by NMR with the superficial liquid velocity measured upstream the test section by electromagnetic flowmeters. The non dimensional distribution of the longitudinal fluid displacement is shown in figure 7(a) and is determined as previously mentioned by inverse Fourier transform of the signal attenuation. By mere scaling arguments (Lemonnier & Leblond, 2007a), it can be shown that the mean non dimensional velocity, $\langle u \rangle_3$, obtained as the first moment of the distribution is related to the superficial velocity by J_L,

$$\frac{\langle u \rangle_3}{\gamma \delta \Delta} = G_Z J_L \tag{11}$$

where G_Z is the maximum value of the gradient strength. Figure 6(a) shows that the linear relationship between $\langle u \rangle_3$ an J_L is correctly followed by experiments. By curve fitting the calibration constant $G_Z \approx 3.5$ G/cm is obtained. When this scaling constant is known, the velocity distributions can be obtained. They are shown in figure 7(b).

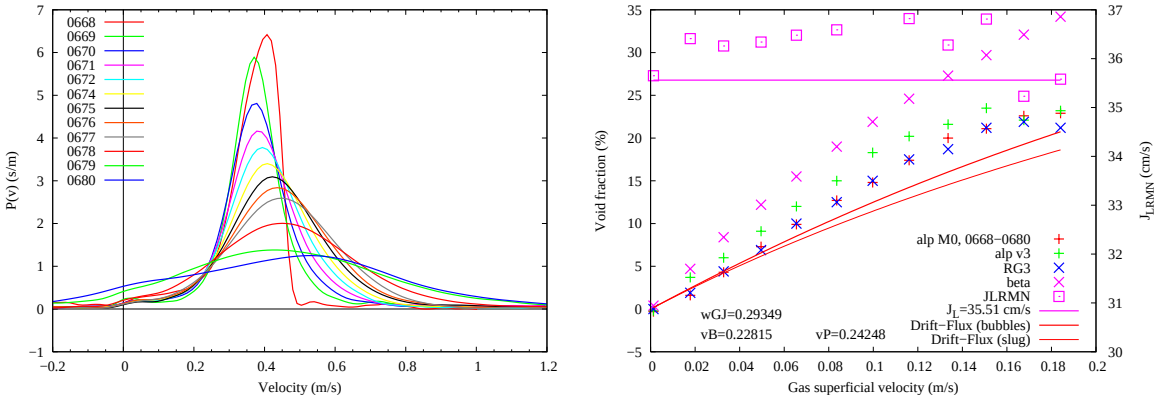

(a) Velocity distributions

(b) Void fraction and mean liquid velocity

Figure 8: Velocity distributions in two-phase flow. $J_L = 35$ cm/s and J_G ranging from 0 to 22 cm/s. Runs 0668 to 0680.

Next, when the spectrometer is calibrated in liquid content and velocity (see Figure 6), two-phase velocity measurements can be obtained by applying the same procedure. In addition, area-averaged void fraction is obtained as the ratio of the magnetization amplitude in two-phase flow to that of single-phase flow with the same transit time in the electromagnet (i.e. (10) estimated with v_L instead of J_L). Two-phase flow velocity distributions are shown in Figure 8(a) and the corresponding mean liquid velocities and void fractions are shown in Figure 8(b). For the two highest void fraction values (runs 0679, 0680, $\alpha > 17\%$) negative velocities are observed. This means that a some locations in the cross section, negative values of the velocity occurred during a significant fraction of observation time. Though the observed flow regime is bubbly flow with bubble clustering, the use of thermal anemometry in these conditions would have been inappropriate since this technique is not sensitive to the velocity sign.

In figure 8(a), for a given liquid flow rate, the increase of mean liquid velocity with the increase of the gas flow rate is clearly shown by the continuous drifting of the distribution towards higher values. In addition the increase of velocity fluctuations widens considerably the distributions when the void fraction increases. From the relationship between the liquid superficial velocity and the mean liquid velocity, v_L, a first void fraction estimate can be obtained

$$J_L = (1 - \alpha_v) v_L \tag{12}$$

These values are shown in Figure 8(b) by the symbols tagged ”alp v3”. These values compare favorably well with those obtained from the magnetization amplitude tagged as ”alp M0”, the former being systematically larger than the latter for reasons not yet understood. These two void fraction estimates compare also well with the direct determination of area void fraction measured by the two-phase pressure change around the measuring volume. Due to technological reasons, the uncertainty of this measurement is quite large ($\pm 1.5\%$) however, these values are fairly consistent with those obtained from the magnetization ratio. These three values are well below the prediction of the homogeneous model tagged as ”beta” in the figure. Finally, the predicted values by the drift-flux model (Ishii & Hibiki, 2006) agree with data showing a maximum deviation of 2.5%. The change of trend between bubbly flow and bubble clustering regime ($\alpha > .17$) is also clear from void fraction measurements as it is from the velocity distributions where the variance of velocity seems to increase drastically beyond this point in agreement with the earlier observations of the turbulence increase reported in Figure 3(b).

As a final check of the NMR measurement, the superficial velocity of the liquid has been calculated from the mean liquid velocity obtained from the velocity distribution and the void fraction estimated from the magnetization amplitude. Those values range between 35 and 37 cm/s as shown in Figure 8(b) to be compared to the expected value 35.5 cm/s. This uncertainty cumulates both the uncertainty of the void

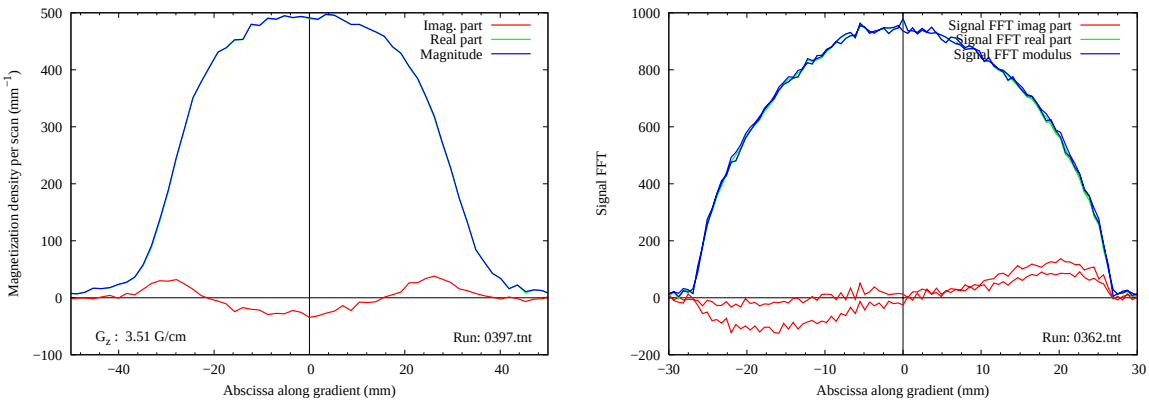

(a) Magnetization along z

(b) Magnetization along x

Figure 9: Magnetization profiles in the longitudinal direction (z and transversal direction, x.

fraction and the velocity and represents our present state of art in determining velocity and composition by NMR.

6 SLICE SELECTION

The data shown up to now was volume-averaged in the so-called control volume. The determination of the shape of the probed volume is a classical discussion in magnetic resonance imaging, MRI (see for example Maneval *et al.* , 1990, for porous media studies). In the previous sections, the utilized procedure can be regarded as a single-pixel image. The sensitivity within this pixel varies both in the longitudinal and the transverse direction. If the PFGSE sequence is applied on a static sample of liquid, it can be shown that the signal $S(g)$ is the Fourier component of the magnetization along the field gradient direction. By inverse Fourier transform, one gets the distribution of the averaged magnetization in a plane perpendicular to this direction. PFGSE sequence is a long procedure which requires taking data at different values of the gradient strength. When time averaging is not necessary, a much faster method consists in analyzing the signal time-decay when a constant field gradient is applied. It can be shown that $S(t)$ is the Fourier transform of the space distribution of magnetization. This is the so-called q- and k-space equivalence (Callaghan, 1991).

Figure 9(a) shows the magnetization distribution in the measuring volume. It is rather homogenous along the pipe axis on a length comparable to the pipe internal diameter (49 mm) and decays rapidly. Figure 9(b) shows the magnetization distribution in the transverse direction. Since the pipe has a circular cross section, the distribution profile is proportional to the length of the chord perpendicular to the pipe diameter: the shape of the pipe is therefore imaged directly by this technique. This shows in addition that the sensitivity of the measurement is homogeneous in the pipe cross section. This was expected from the coils design (Javelot, 1994).

By applying a static field along the pipe direction, the resulting fluid magnetization is also along the pipe axis and therefore cannot be detected. A short RF pulse is usually applied to tilt the magnetization at right angle with the pipe axis. It can be shown that the magnetization is no longer static but rotates around the static field direction with a frequency proportional to the static field. Varying magnetization induces a voltage into the RF coil that can be used for the detection of the NMR signal *S*. The measuring volume is therefore the fraction of space where the magnetization has been tilted and therefore can be detected.

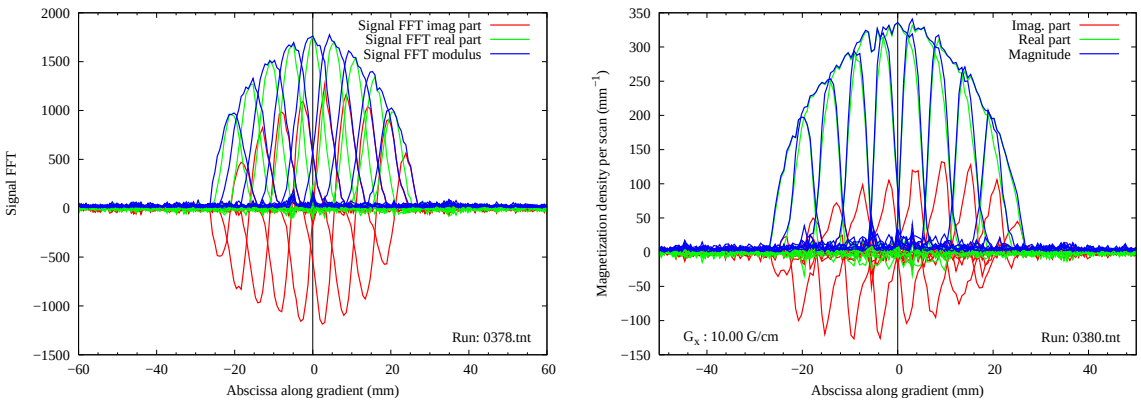

(a) X-Gaussian selection, slice 10 mm

(b) X-Sinc selection, slice 12 mm

Figure 10: Magnetization distributions after various X-slice selections. (a) Gaussian RF pulse, (b) Sinc, 5 lobes, RF pulse.

By varying the shape, length and frequency of the RF pulse an applying simultaneously a gradient pulse, one can vary the shape and width of the of the probed volume (see for example Hoult, 1979, for a detailed description of this relationship). The figure 10(a) shows the implementation of the selection (9 pixels) with a Gaussian pulse. Magnetization profile in stand fluid is an image of the sensitivity distribution within each pixel. A simple approximate theory (Hoult, 1979, first order) shows that the sensitivity distribution is the Fourier transform of the RF pulse envelop. A Gaussian being invariant through a Fourier transform, a Gaussian sensitivity in space results. If a hat selection is desired, theory tells that a sinc ($\sin x/x$) selection should be used. A few, 3 to 5, lobes are used in practice and Figure 10(b) shows the result of a 5-lobes sinc RF pulse. The resulting sensitivity profile is a hat function. More precisely, the sensitivity profile is the product of a "free space" sensitivity distribution than can be calculated by solving the Bloch equations (Hoult, 1979) and the "natural sensitivity of the RF coil as shown in figure 9.

Barberon & Leblond (2001) used this selection technique combined with the PFGSE to get the area averaged void fraction and liquid velocity distribution along a slug bubble. The thickness of the slice was approximately 5 mm which is small compared to a typical Taylor bubble length of 5 to 10 diameter. Clearly when applied to our flow with a lateral selection gradient, it is clear that detailed information on the profiles can be obtained in addition to the mean values. This may require solving a inverse problem of Abel type which is not that difficult since many solutions exist to this problem (Adanson *et al.* , 1978, Knill, 1994).

It is of interest to consider that the space filtering introduced by the NMR probe sensitivity distribution provides velocity and void fraction values that are space-filtered and time averaged. Since the relation between the signal and velocity *is linear*, the two averages commutes which is not the case with thermal anemometry. Furthermore, The measured quantities are very similar to those that appear within space-filtered of LES like models. To our knowledge no other method provides such an easy access to these mean values.

7 CONCLUSIONS AND FUTURE WORK

It has been shown that NMR can be used to measure area-averaged void fraction and liquid velocity in two-phase flow. This was already shown with the same equipment by Javelot (1994). In addition turbulent eddy viscosity can be obtained from the analysis of the magnetization decay and using an analysis based on the classical approach of Stejskal & Tanner (1965). Since the diffusion limit is in

general not reached within the measurement time scale, it is necessary to reconsider the theory with a time varying diffusivity (Taylor, 1921) and the new result agrees with the data and a the former analysis of single-phase turbulent flow by Gatenby & Gore (1994). When the new analysis is applied to two-phase flow, it seems now fully consistent with the former analysis of Serizawa *et al.* (1975b) who utilized a thermal method. The sample data analyzed here seems to be consistent with the former analysis of these authors and agree with the earlier theoretical estimates of Sato & Sadatomi (1981). NMR data, provides the correlation time of the velocity fluctuations which can be used to justify the choice of the averaging time of the balances equations.

Finally, future work will be dedicated to implement the present analysis together with the selection technique leading to a possible access to distribution of these quantities within the cross section.

REFERENCES

Adanson, P., Cheminat, B., & Halbique, A. M. 1978. Résolution de l'équation intégrale d'Abel : Application à la spectrométrie des plasmas. *J. Phys D: Apll. Phys.*, **11**, 7209–215. ⇒.

Barberon, F., & Leblond, J. 2001. Intermittent two-phase flow study by NMR. *C. R. Acad. Sci. Paris, Chemistry*, **4**, 853–856. ⇒.

Bergles, A.E, Collier, J. G., Delhaye, J. M., Hewitt, G. F., & Mayinger, F. 1981. *Two-phase flow and heat transfer in the power and process industries*. McGraw Hill.

Callaghan, P. T. 1991. *The principles of magnetic resonance microscopy*. Oxford Science Publications.

Carr, H. Y., & Purcell, E. M. 1954. Effects of diffusion on free precession in nuclear magnetic resonance experiments. *Phys. Rev*, **94**(3), 630–638. ⇒.

Daalmans, A. C. L. M., Portela, L. M., & Mudde, R. F. 2007. Development of a NMR multiphase flowmeter. *In: Proc. 6th International Conference on multiphase flows, ICMF2007*. ⇒.

Delhaye, J. M., Giot, M., & Riethmuller, M. L. 1981. *Thermohydraulics of two-phase systems for industrial design and nuclear engineering*. McGraw Hill.

Fukushima, E. 1999. Nuclear magnetic resonance as a tool to study flow. *Annu. Rev. Fluid Mech.*, **31**, 95–123. ⇒.

Gatenby, J. C., & Gore, J. C. 1994. Characterization of turbulent flows by NMR measurements with pulsed field gradients. *Journal of Magnetic Resonance, A*, **110**, 26–32. ⇒.

Grossetête, C. 1995. *Caractérisation expérimentale et simulation de l'évolution d'un écoulement à bulles ascendant dans une conduite verticale*. Ph.D. thesis, Ecole Centrale Paris.

Hoult, D. I. 1979. The solution of Bloch Equations in the presence of varying B1 field - An approach to selective pulse analysis. *J. Mag. Resonance*, **35**, 69–86. ⇒.

Ishii, M., & Hibiki, T. 2006. *Thermo-fluid dynamics of two-phasse flows*. Springer.

Javelot, S. 1994. *Réalisation d'un dispositif utilisant la RMN pour caractériser les écoulements multiphasiques*. Ph.D. thesis, Université Paris 6. ⇒.

Kataoka, I. 1986. Local instant formulation of two-phase flow. *Int. J. Multiphase Fow*, **12**(5), 745–758. ⇒.

Kataoka, I., & Serizawa, A. 1989. Basic equations of turbulence in gass-liquid two-phase flow. *Int. J. Multiphase Fow*, **15**(5), 843–855. ⇒.

Knill, O. 1994. Diagonalization of Abel's integral operator. *Siam J. Appl. Math.*, **54**(5), 1250–1253.

Leblond, J., Benkedda, Y., & Oger, L. 1994. Two-phase flow by pulsed field gradient spin echo NMR. *Meas. Sci. Technol.*, **5**, 426–434. ⇒.

Leblond, J., Javelot, S., Lebrun, D., & Lebon, L. 1998. Two-phase flow characterization by nuclear magnetic resonance. *Nuclear Engineering and Design*, **184**, 229–237. ⇒.

Lemonnier, H., & Leblond, J. 2007a. Application of NMR to fluid flow measurements. *In: Proc. 12th ANS/THD Nuclear Reactor Thermal-Hydraulics, Nureth-12*. Paper 61, ⇒.

Lemonnier, H., & Leblond, J. 2007b. Two-phase flow velocity and void fraction measurements revisited by using nuclear magnetic resonance. *In: Proc. 6th International Conference on multiphase flows, ICMF2007*. ⇒.

Liu, T. J., & Bankoff, S. G. 1993. Struture of air water bubbly flow in a vertical pipe-I. liquid mean veocity and trbulence measurements. *Int. J. Heat Mass Transfer*, **36**(4), 1049–1060. ⇒.

Maneval, J. E., McCarhy, M. J., & Whitaker, S. 1990. Use of NMR as an experimental probe in multiphase systems: determination of the instrument weight function for measurements of liquid-phase volume fractions. *Water Resources Res.*, **26**(11), 2807–2816. ⇒.

Mimouni, S., Boucker, M., Laviéville, J., Guelfi, A., & Bestion, D. 2008. Modelling and computation of cavitation and boiling bubbly flows with the NEPTUNE-CFD code. *Nuclear Engineering and Design*, **238**(3), 680–692. ⇒.

Rodriguez, A. O. 2004. Principles of magnetic resonance imaging. *Rev. Mex. Fisica*, **50**(3), 272–286. ⇒.

Sato, Y., & Sadatomi, M. 1981. Momentum and heat transfer in two-phase bubbly flow-I. *Int. J. Multiphase Flows*, **7**, 167–177. ⇒.

Sato, Y., & Sekoguchi, K. 1975. Liquid velocity distribution in two-phase bubble flow. *Int. J. Multiphase Flows*, **2**, 75–95. ⇒.

Sato, Y., Sadatomi, M., & Sekoguchi, K. 1981. Momentum and heat transfer in two-phase bubbly flow-II: A comparison between experimental data and theoretical calculations. *Int. J. Multiphase Flows*, **7**, 179–190. ⇒.

Serizawa, A., Kataoka, I., & Michiyoshi, I. 1975a. Turbulence structure of air water bubbly flow- I. measuring techniques. *Int. J. Multiphase Flow*, **2**, 221–233. ⇒.

Serizawa, A., Kataoka, I., & Michiyoshi, I. 1975b. Turbulence structure of air water bubbly flow- III. transport properties. *Int. J. Multiphase Flow*, **2**, 247–259. ⇒.

Stejskal, E. O., & Tanner, J. E. 1965. Spin diffusion measurements: spin echoes in the presence of a time dependent field gradient. *Journal of Chemical Physics*, **42**(1), 288–292. ⇒.

Taylor, G. I. 1921. Diffusion by continuous movements. *Proc. London Math Soc.*, **20**, 196–212. ⇒.

Tennekes, H., & Lumley, J. L. 1972. *A first course in turbulence*. MIT Press. ⇒.